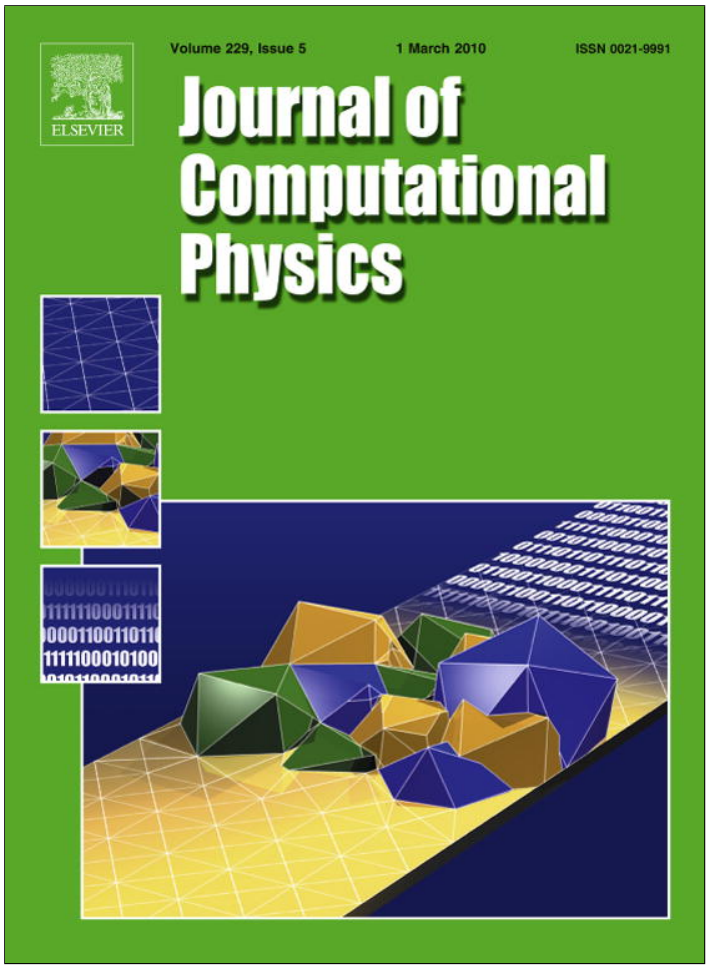

Journal of Computational Physics 229 (2010) 1879–1896

Contents lists available at ScienceDirect

Journal of Computational Physics

journal homepage: www.elsevier.com/locate/jcp

# Nonreflecting boundary conditions for discrete waves

A. Carpio *, B. Tapiador

*Dep. Matemática Aplicada, Fac. Matemáticas, Universidad Complutense de Madrid, 28040 Madrid, Spain*

ARTICLE INFO

*Article history:*
Received 19 December 2008
Received in revised form 6 October 2009
Accepted 9 November 2009
Available online 14 November 2009

*Keywords:*
Nonreflecting boundary conditions
Green's functions
Lattice models
Discrete wave equations
Transparent boundary conditions
Absorbing boundary conditions
Dirichlet-to-Neumann operators
Molecular dynamics

ABSTRACT

We introduce a new class of nonreflecting boundary conditions for lattice models, which minimizes reflections at artificial boundaries. Exact integrodifferential boundary conditions for finite chains and half-spaces are obtained by means of Green's functions for initial value problems. Truncating the resulting integrals in time, we obtain absorbing boundary conditions. Numerical tests illustrate the ability of these conditions to suppress reflections.


## 1. Introduction

In many physical and biological problems waves propagating in discrete lattices play a key role: motion of dislocations [21] or cracks [40] in crystalline materials, atoms adsorbed on a periodic substrate [14], motion of electric field domains in semiconductor superlattices [11], pulse propagation through myelinated nerves [2] or cardiac cells [31]...Computing in a reliable way waves propagating in large oscillator networks is a complex task due to spurious oscillations and pinning. A common procedure is to truncate the lattice, select some artificial boundary conditions and solve the resulting system of equations. A poor choice of boundary conditions may change the qualitative behavior of the solutions due to spurious reflections, as shown in Figs. 1 and 2.

The problem of finding artificial boundary conditions may be formulated in several related, but different, contexts: partial differential equations with continuous time and space variables, discretizations of partial differential equations, spatially discrete systems which take the form of large systems of ordinary differential equations, and discretizations in time of spatially discrete systems. In this paper we address the last two frameworks. For the last decades, most work on nonreflecting boundary conditions has focused on wave propagation in continuum media. The interest in deriving nonreflecting boundary conditions for spatially discrete systems has grown recently, due to the need of simulating atomic or cellular systems in nanotechnology and bioengineering.

Some spatially discrete models can be seen as spatial discretizations of partial differential equations by the method of lines. Their discretizations in time may look like discretizations in time and space of partial differential equations. However,

* Corresponding author. Tel.: +34 91 3944479; fax: +34 91 3944613.
*E-mail address:* ana_carpio@mat.ucm.es (A. Carpio).

0021-9991/$ - see front matter © 2009 Elsevier Inc. All rights reserved.
doi:10.1016/j.jcp.2009.11.013

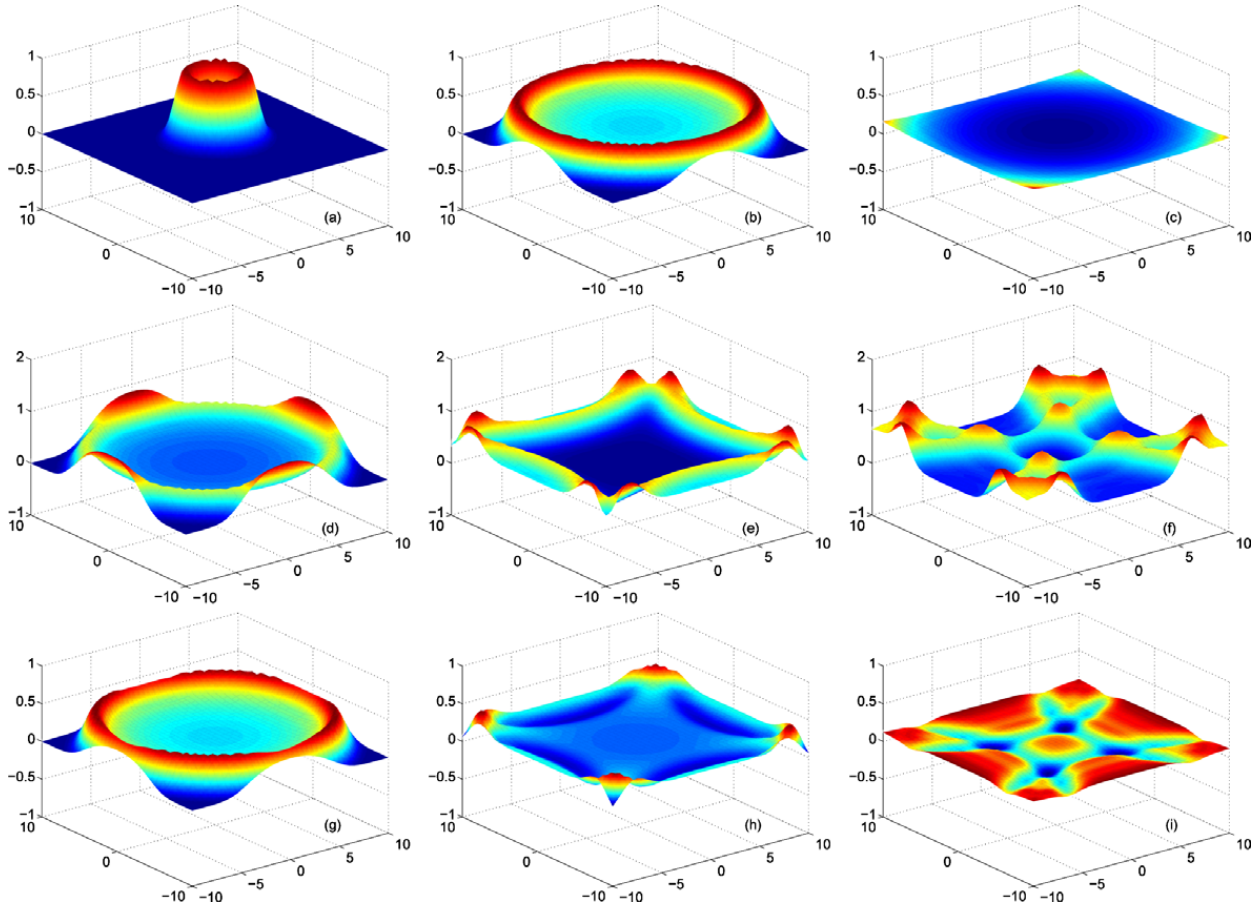


**Fig. 1.** (a) Outgoing wave and (b), (c) its true evolution inside the computational domain, governed by a wave equation. Effect of the artificial boundary: (d)–(f) with periodic boundary conditions and (g)–(i) with absorbing boundary conditions for wave equations. Numerical solutions are computed in a square lattice using a second order scheme with steps $\Delta t = 0.28$ and $\Delta x = 0.5$.

there is an important difference: there is no parameter representing a spatial step which tends to zero. The size of the parameters is fixed (except for the time step) and this may change the qualitative behavior of the solutions we want to approximate, see Figs. 1 and 2. These figures show the evolution of a gaussian when its dynamics is governed by a wave equation (Fig. 1) and a spatially discrete wave equation (Fig. 2). We are not interested in suppressing the dispersive effects or oscillations generated by the spatially discrete structure, which are not spurious artifacts due to spatial discretization, but features inherent to our problem. Moreover, the discrete spatial structure is fixed and cannot be selected to match some particular boundary conditions.

Three types of boundary conditions are commonly employed in continuum problems. Exact (or transparent) nonreflecting boundary conditions make the truncated problem equivalent to the full system. If found, they are usually nonlocal and difficult to implement, see [19,25,22,23] for wave equations. If wave motion arises entirely within the computational domain and outside it there are no mechanisms causing reflection back inside, the solution near the boundary consists of outgoing waves. Thus, the artificial boundary condition should simulate an outward radiation of energy. By approximating the kernels in the exact nonreflecting boundary conditions, we get local absorbing boundary conditions. They are easier to handle but often give rise to long time instability or ill posed problems, see [19,20,26,41] for acoustic and elastic waves. In general, one cannot construct nonreflecting boundary conditions unless the behavior of the solution at infinity is known. Alternative radiation boundary conditions based on asymptotic expansions of the far field of the solutions may be proposed, see [6–8] for wave-like equations and compressible flows. The third possibility consists in introducing a perfectly matched layer outside the computational domain. This idea works for electromagnetic waves [10] and extensions to fluid problems or elastic waves have been tried [3,15]. However, instabilities have been reported in anisotropic media [9].

For computational purposes, all the nonreflecting boundary conditions derived for continuum media must be discretized and combined with discretizations of the equations. The dispersion laws of continuous problems and their discretized counterparts being different, most schemes generate some kind of reflection, see [34] and references therein. In practice, one must find discretely nonreflecting boundary conditions for the discretized equations, which suppress reflections inside the computational domain generated at the artificial boundaries and also spurious waves originated by the dispersive nature of the discrete schemes. Different approaches to deriving nonreflecting boundary conditions for fully discretized wave equations are discussed in [27,28,35]. In [34], exact boundary conditions are found for fully discretized

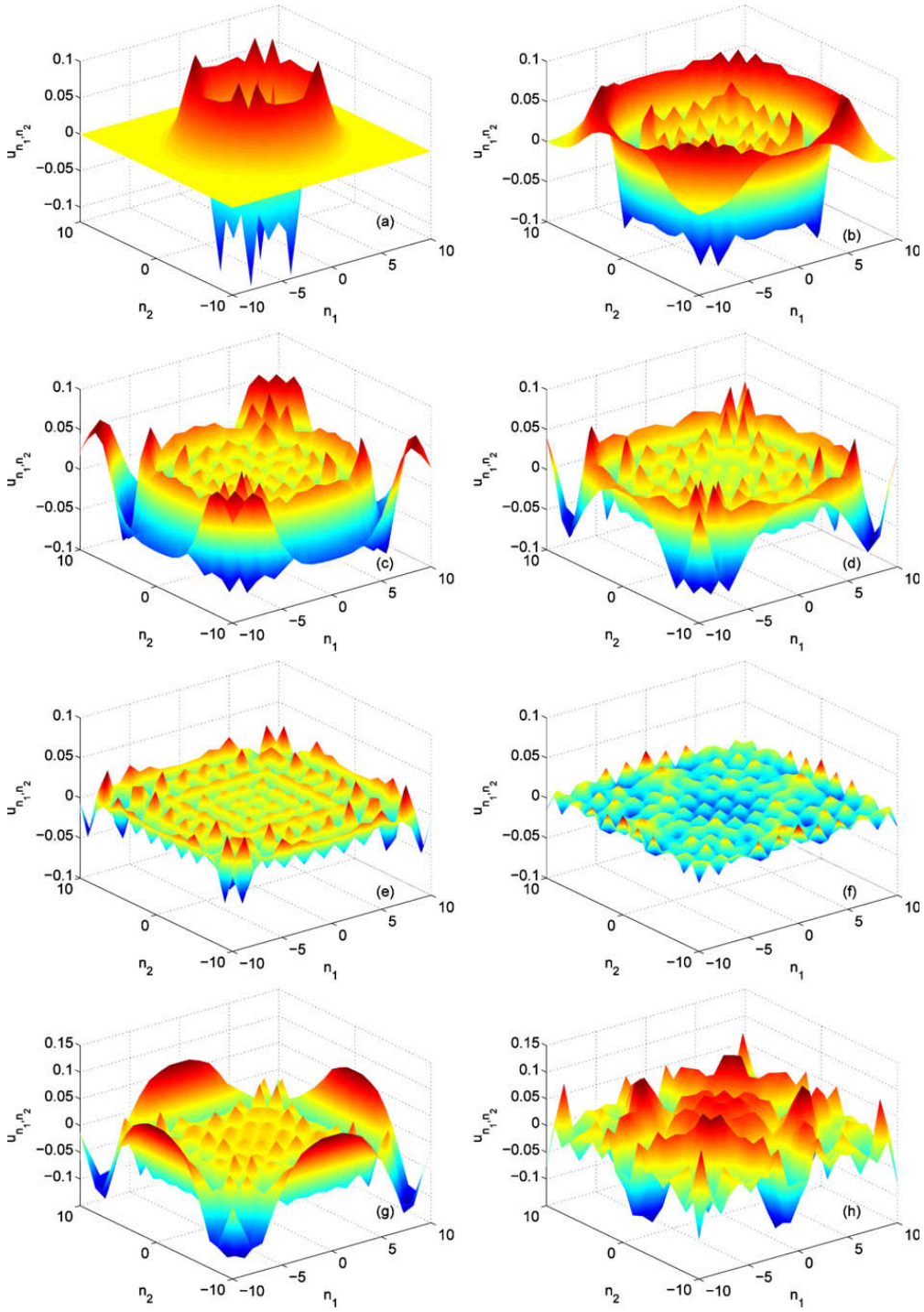


**Fig. 2.** Outgoing wave governed by (32) with $D = 1$ at times $t = 5$ (a), $t = 10$ (b), $t = 13$ (c), $t = 15$ (d), $t = 20$ (e) and $t = 30$ (f). In (a)–(e), the true solution is indistinguishable from the numerical solution, computed using the second order scheme described in Section 4.1.4 and imposing a truncated nonreflecting boundary condition on the walls. Parameters are $\tau = 5, M = 5$ and $h = 0.01$. (g) and (h) show the wave at times 15 and 30 for zero Dirichlet boundary conditions.

linear hyperbolic systems and approximate boundary conditions are proposed for semidiscrete systems. [4] derives exact boundary conditions for fully discretized wide angle parabolic equations. Transparent conditions for Schrödinger equations discretized in time are presented in [37] and references therein.

The issue of suppressing reflections at artificial boundaries arises in many other fields, in particular, when studying atomic scale processes in crystalline solids by means of molecular dynamics (MD) simulations. In numerical simulations of nanoindentation experiments, for instance, atomic size effects are only relevant at a small region below the tip of the indenter, where defects are nucleated. MD models are employed in a small region and then truncated at an artificial boundary or coupled with macroscopic descriptions (finite elements typically), see [39] for a survey of techniques. A Green's function method

to dynamically couple the two regions by means of a time dependent boundary condition has been developed in [12]. The response of the outer linear domain is included in the form of a generalized Langevin [1] equation with a convolution integral over the velocities in the computational domain. The convolution kernel is computed using a MD simulation on a larger domain. Nonreflecting boundary conditions for atomic simulations in crystals based on the lattice dynamics Green's functions have been proposed in [30]. In [16], an alternative lattice Green's function based methodology is introduced to evaluate the dynamical properties of concurrent elastic multiscale models. An artificial nonreflecting interface for lattices is constructed in [17] by employing time integration formulas that suppress reflections. Their technique is a reformulation of the idea of absorbing boundary conditions for coupled systems. Other attempts to minimize boundary reflections include viscous ad hoc damping [29], rely on an approximate description of coupling across a domain boundary [33] or are based on direct minimization [18].

In this paper we propose nonreflecting boundary conditions for one dimensional chains of coupled oscillators. The idea is to express the response of the exterior domain to changes in the computational domain as a non local term in time involving Green's functions for spatially discrete initial value problems, that act as memory kernels. The resulting artificial boundary conditions are exact for linear systems. We suggest a procedure to approximate the time integrals, reducing the computational cost without generating long time instabilities. This strategy yields effective absorbing boundary conditions, which involve linear combinations of values of the solution at the boundary points at previous times. Combining with symplectic solvers for systems of ordinary differential equations, we obtain schemes of order two and four. Numerical tests for harmonic chains illustrate their ability to suppress reflections.

This idea extends to spatially discrete wave and Klein Gordon equations in higher dimensions and might be exploited for MD simulations in crystals of arbitrary symmetry. We obtain simple expressions for the Green's functions of initial value problems in half-spaces by exploiting the structure of spatially discrete wave equations, which allows for odd extensions to the whole space. A slight modification allows to formulate exact boundary conditions for vector problems. Previous work on crystals governed by vector lattice models [30] used the lattice Green's functions. This resulted in more complex closures, kernels and algorithms. In spatially discrete wave equations, for instance, our strategy avoids inverting Laplace transforms. For finite boxes we construct approximate boundary conditions truncating the exact boundary conditions for half-spaces, which produces good numerical results.

For scalar problems set in simple geometries, we may draw an analogy with the Dirichlet-to-Neumann technique [23,24] for wave equations. Known the boundary values for a time dependent problem set in a half-space, we find a formula for the values at a neighboring interface, which allows to close the system. As a subproduct, expressions for discrete versions of normal derivatives in terms of time integrals of the values at the boundary follow. In vector problems the analogy is lost: at each fixed time our formulas involve not only known values at the boundary, but also values at the neighboring interface for previous times. In general crystals we work with non orthogonal coordinates. It becomes pointless to look for connections with derivatives.

The paper is organized as follows. In Section 2 we obtain the exact boundary conditions for a one dimensional lattice. Section 3 describes some numerical tests. In Section 4 we extend the method to higher dimensions. Finally, Section 5 presents our conclusions.

## 2. Nonreflecting boundary conditions in one dimension

We consider a one dimensional chain obeying the dimensionless equations:

$$Mu_n'' = V'(u_{n+1} - u_n) - V'(u_n - u_{n-1}) - W'(u_n), \quad n \in \mathbb{Z}. \tag{1}$$

Here, $u_n$ represents the dimensionless displacement of the $n$-th atom with respect to its equilibrium position. $M > 0$ is its dimensionless mass. $V$ is the interatomic potential and $W$ the on-site potential. Possible defects are concentrated in the region $|n| \ll N$. Near $N$, we may linearize (1) to obtain:

$$u_n'' = D(u_{n+1} - 2u_n + u_{n-1}) - Au_n, \quad D = \frac{K_1}{M}, \quad A = \frac{K_2}{M} > 0. \tag{2}$$

If $A = 0$, (2) is a spatially discrete wave equation. If $A > 0$, we have a spatially discrete Klein–Gordon equation. We locate an artificial boundary at $|n| = N$ and seek an exact boundary condition for (2). This means that solving the inner problem in $|n| \leqslant N$ with that boundary condition produces the same result in the inner region as solving (2) everywhere. Exact boundary conditions for (2) become approximate boundary conditions for (1) due to linearization. The first step in deriving our boundary conditions is to compute the Green's function for linear initial value problems.

### 2.1. Green's functions

We want to find an integral representation of the solution of the problem:

$$u_n'' = D(u_{n+1} - 2u_n + u_{n-1}) - Au_n + f_n, \tag{3}$$

$$u_n(0) = u_n^0, \quad u_n'(0) = u_n^1, \tag{4}$$

with $D = \frac{K_1}{M}$, $A = \frac{K_2}{M} > 0$. Firstly, we get rid of the difference operator by using the generating functions $p(\theta,t), f(\theta,t)$:

$$p(\theta,t) = \sum_n u_n(t)e^{-in\theta}, \quad f(\theta,t) = \sum_n f_n(t)e^{-in\theta}. \tag{5}$$

Differentiating $p$ with respect to $t$ and using (3), we see that $p$ solves the ordinary differential equation:

$$p''(\theta,t) + \omega(\theta)^2 p(\theta,t) = f(\theta,t), \quad \omega(\theta)^2 = 4D\sin^2\left(\frac{\theta}{2}\right) + A. \tag{6}$$

Initial conditions for $p$ follow from those for $u_n$. The solution $p$ of (6) depends on the roots of the polynomial $r^2 + \omega(\theta)^2 = 0$:

$$p(\theta,t) = p(\theta,0)\cos(\omega(\theta)t) + p'(\theta,0)\frac{\sin(\omega(\theta)t)}{\omega(\theta)} + \int_0^t \frac{\sin(\omega(\theta)(t-s))}{\omega(\theta)} f(\theta,s)ds, \tag{7}$$

and $u_n(t)$ is recovered inverting the discrete Fourier transform:

$$u_n(t) = \int_{-\pi}^{\pi} \frac{d\theta}{2\pi} e^{in\theta} p(\theta,t). \tag{8}$$

Formula (8) can be rewritten as:

$$u_n(t) = \sum_k \left[ G_{nk}(t)u_k'(0) + \frac{dG_{nk}}{dt}(t)u_k(0) \right] + \int_0^t \sum_k G_{nk}(t-s)f_k(s)ds \tag{9}$$

where

$$G_{nk}(t) = \int_{-\pi}^{\pi} \frac{d\theta}{2\pi} \frac{e^{i(n-k)\theta}}{\omega(\theta)} \sin(\omega(\theta)t). \tag{10}$$

Green's functions for hamiltonian chains were computed by Schrödinger in [38]. Their properties are analyzed in detail in [5]. Dissipative chains are studied in [13]. Convergence of the sums in (9) follows from the spatial decay of the Green's functions. Integrating by parts in (10) and using the periodicity of $e^{i(n-k)\theta}$ we see that $G_{nk}$ decays like $|n-k|^p$ for any $p > 1$. Notice that $\omega(\theta)$ being even with respect to $\theta$, the Green's function (10) is real.

### 2.2. Exact nonreflecting boundary conditions in a half-space

We wish to solve (2) for $n \geqslant 0$, placing an artificial boundary at $n = 0$. Thus, we need a boundary condition to compute $u_0(t)$. In principle,

$$u_0'' = D(u_1 - 2u_0 + u_{-1}) - Au_0 + f_0, \tag{11}$$

but $u_{-1}(t)$ is unknown unless we solve (2) for $n \leqslant 0$ with boundary data $u_0(t)$ at $n = 0$ and compute $u_{-1}(t)$. Below, we describe a strategy to obtain an explicit expression for $u_{-1}(t)$. Let us rewrite (3) at $n = -1$ as:

$$\frac{d^2u_{-1}}{dt^2} = D(0 - 2u_{-1} + u_{-2}) - Au_{-1} + f_{-1} + Du_0. \tag{12}$$

Assuming we know $u_0(t)$, the problem (3)–(4) for $n \leqslant 0$ with boundary condition $u_0(t)$ can be extended to the whole space setting:

$$v_n = \begin{cases} -u_{-n} & n > 0, \\ 0 & n = 0, \\ u_n & n < 0. \end{cases} \tag{13}$$

The extension $v_n$ solves:

$$\begin{aligned} &v_n'' = D(v_{n+1} - 2v_n + v_{n-1}) - Av_n + g_n, \\ &v_n(0) = v_n^0, \quad v_n'(0) = v_n^1, \end{aligned} \tag{14}$$

for all $n$, where $v_n^0$ and $v_n^1$ are odd extensions of $u_n^0$ and $u_n^1$ defined as in (13). The source $g_n$ is obtained extending $f_n + D\delta_{n,-1}u_0$ in a similar way:

$$g_n = \begin{cases} -f_{-n} & n > 1, \quad -f_{-1} - Du_0 \quad n = 1, \\ 0 & n = 0, \\ f_n & n < -1, \quad f_{-1} + Du_0 \quad n = -1. \end{cases} \tag{15}$$

Notice that we have included the boundary condition $u_0$ as a force acting on $v_{-1} = u_{-1}$ to allow for an odd extension with zero boundary condition $v_0 = 0$. Using (9) and the symmetry of the data:

$$u_n(t) = v_n(t) = \sum_{k<0}\left[\mathscr{G}_{nk}(t)u_k'(0) + \frac{d\mathscr{G}_{nk}}{dt}(t)u_k(0)\right] + \int_0^t \sum_{k<0}\mathscr{G}_{nk}(t-s)(f_k(s) + D\delta_{k,-1}u_0(s))ds, \quad n<0, \tag{16}$$

where $\mathscr{G}_{nk} = G_{n,k} - G_{n,-k}$ is the Green's function for the half space $n < 0$ with zero boundary condition at $n = 0$. The desired formula for $u_{-1}$ follows:

$$\begin{aligned} u_{-1}(t) &= r_{-1}(t) + D\int_0^t \mathscr{G}_{-1-1}(t-s)u_0(s)ds, \\ r_{-1}(t) &= \sum_{k<0}\left[\mathscr{G}_{-1k}(t)u_k'(0) + \frac{d\mathscr{G}_{-1k}}{dt}u_k(0) + \int_0^t \mathscr{G}_{-1k}(t-s)f_k(s)ds\right]. \end{aligned} \tag{17}$$

The term $r_{-1}(t)$ represents the contribution of the data in the outer region. Our boundary condition at $n = 0$ takes the form:

$$u_0'' = D\left(u_1 - 2u_0 + D\int_0^t \mathscr{G}_{-1-1}(t-s)u_0(s)ds\right) + Dr_{-1} + f_0, \tag{18}$$

where the kernel is:

$$\mathscr{G}_{-1-1}(t) = \int_{-\pi}^{\pi}\frac{d\theta}{2\pi}\frac{1-e^{-2i\theta}}{\omega(\theta)}\sin(\omega(\theta)t) = \int_{-\pi}^{\pi}\frac{d\theta}{2\pi}\frac{1-\cos(2\theta)}{\omega(\theta)}\sin(\omega(\theta)t). \tag{19}$$

### 2.3. Exact boundary conditions for a finite chain

Let us truncate our computational domain to a finite chain $|n| \leqslant N$. We wish to impose nonreflecting boundary conditions at $n = \pm N$. Using the results derived in the previous section, we would set:

$$\frac{d^2u_{\pm N}}{dt^2} = D\left(u_{\pm(N-1)} - 2u_{\pm N} + D\int_0^t \mathscr{G}_{-1-1}(t-s)u_{\pm N}(s)ds\right) + Dr_{\pm(N+1)} + f_{\pm N}, \tag{20}$$

$$\begin{aligned} u_{\pm(N+1)}(t) &= r_{\pm(N+1)}(t) + D\int_0^t \mathscr{G}_{\pm1,\pm1}(t-s)u_{\pm N}(s)ds, \\ r_{\pm(N+1)}(t) &= \sum_{N\mp k<0}\left[\mathscr{G}_{\pm1,k\mp N}(t)u_k'(0) + \frac{d\mathscr{G}_{\pm1,k\mp N}}{dt}u_k(0) + \int_0^t \mathscr{G}_{\pm1,k\mp N}(t-s)f_k(s)ds\right]. \end{aligned} \tag{21}$$

The kernel $\mathscr{G}_{1,1} = \mathscr{G}_{-1,-1}$ is given by (19). Once we have derived our boundary conditions, a few remarks are in order:

- Unlike many nonreflecting boundary conditions for continuous waves, no assumptions on the support of the data are made. We do not assume the data to have compact support contained in the computational domain.
- The series can be truncated to a finite range of $k$ using the decay properties of $G_{\pm1,k}(t)$ as $|k|$ grows.
- When the initial data and the source are compactly supported in the computational domain, $r_{\pm(N+1)}(t) = 0$ and the boundary conditions involve only $u_{\pm N}$ and its closest interior neighbor. Still, the boundary condition is non local in time due to the presence of an integral term.
- The source $r_{\pm(N+1)}(t)$ represents the interaction with the external medium. The expressions for $r_{\pm(N+1)}(t)$ in (21) can be replaced with the solution of finite element or meshless schemes for the outer problems, which can be more efficient in higher dimensions. We would obtain an hybrid multiscale scheme coupling an atomic model with a discretized continuum description.
- Friction terms $\frac{\partial u_{\pm N}}{\partial t}$ are commonly introduced in the equations near the extremes of the lattices, in an heuristic attempt (often unsuccessful or uncontrolled) to reduce reflections produced by arbitrary choices of the boundary conditions. Time derivatives are then discretized as linear combinations of values of $u_{\pm N}$ at earlier times. The integral term appearing in our boundary conditions (20) is also discretized as a more complex linear combination of values of $u_{\pm N}$ at earlier times. It can be interpreted as a friction term generated by the tails of the chain. Comparing with the approximate boundary conditions for semiscrete hyperbolic systems proposed in [34], our nonreflecting conditions involve values at the boundary points at previous times and not values at all the points for the current time.
- At each wall, we express $u_{\pm(N+1)}$ in terms of the data $u_{\pm N}$. Thus, we know the differences $u_{\pm(N+1)} - u_{\pm N}$, which are discrete versions of normal derivatives. We have computed the spatially discrete time dependent Dirichlet-to-Neumann operators [23] in the exterior domains $n < -N$ and $n > N$.

## 3. Numerical results

In this section we test the ability of the boundary conditions derived in the previous section to suppress reflections at artificial boundaries.

### 3.1. Discretization

The simplest schemes use a second order approximation for the time derivative:

$$\frac{d^2u_n(t)}{dt^2} = \frac{u_n(t+h) - 2u_n(t) + u_n(t-h)}{h^2} + O(h^2). \tag{22}$$

Since the kernels $\mathscr{G}_{-1,-1}(t-s)$ oscillate and decay as $t-s$ grows [5], we may truncate the integrals appearing in (20) to an interval $[t-\tau, t], \tau \geqslant 0$, and apply the composite trapezoidal rule (order 2) to discretize the resulting integrals. The final scheme takes the form:

$$u_n^{j+1} - 2u_n^j + u_n^{j-1} = h^2 D\left(u_{n+1}^j - 2u_n^j + u_{n-1}^j\right) - Ah^2 u_n^j, \quad -N < n < N, \tag{23}$$

$$u_{\pm N}^{j+1} - 2u_{\pm N}^j + u_{\pm N}^{j-1} = h^2 D\left(u_{\pm(N-1)}^j - 2u_{\pm N}^j + u_{\pm(N+1)}^j\right) - Ah^2 u_{\pm N}^j, \tag{24}$$

for $j = 1, 2, \ldots$, where

$$u_{\pm(N+1)}^j = Dh\left(\sum_{\ell=0}^{\min(j,n_\tau)} c_\ell K(t_\ell) u_{\pm N}(t_j - t_\ell)\right) + r_{\pm(N+1)}^j, \tag{25}$$

with $\tau = n_\tau h, r_n^j = r_n(t_j), c_0 = c_{n_\tau} = 1/2, c_\ell = 1, \ell = 1, \ldots, n_\tau - 1$ and $t_\ell = \ell h, \ell = 0, 1, 2, \ldots$. If we compute the integrals over $[0, t_j]$, then $n_\tau = j$ and $\tau = t_j$ grow from one step to the next. Otherwise, they are fixed.

The weights $K(t_\ell) = \mathscr{G}_{-1,-1}(t_\ell), \ell = 0, \ldots, n_\tau$, are evaluated once and then stored. These weights must be calculated with enough precision to avoid spurious oscillations or instabilities. Notice that the integrand in (19) is oscillatory, and the frequency of the oscillations increases with $t_\ell$. As a result, $K(t_\ell)$ tends to zero as $t_\ell$ grows. We have used Matlab packages based on adaptive Lobatto quadrature with tolerance $10^{-6}$. The precision should be adapted to the cut-off value $\tau$, to avoid loosing all the significative digits past a certain time. This is the most expensive step in our scheme. Once the weights have been stored, the cost is reduced to evaluating (23)–(25).

The presence of integrals makes constant time step schemes a natural choice for this problem. However, the evaluation of a convolution integral at each time step might render the cost too high. The decaying nature of our kernels prevents this. In our tests, $n_\tau$ is small enough to allow for a fast straightforward computation of the sums in (25). The higher order schemes developed in Section 3.3 reduce the number of convolutions to be computed by increasing the time step. Other acceleration strategies are discussed in Section 4.1.4.

### 3.2. Numerical tests

A series of numerical experiments have been performed to test the efficiency of our boundary conditions. We compare solutions of (2) computed in two lattices of increasing size $[-N_1, N_1], [-N_2, N_2], N_1 \ll N_2$, the first one being several times smaller than the second one. In the biggest lattice we impose zero Dirichlet boundary conditions. We use gaussians with compact support in the smaller lattice as initial data, so that there is no interaction with the boundary of the large lattice during the computing time and the solution can be taken as exact. Numerical solutions are generated with the scheme (23)–(24) and boundary conditions $u_{\pm(N_2+1)} = 0$.

Fig. 3 shows a sequence of snapshots superimposing solutions obtained in the small lattice for three different boundary conditions and the reference 'exact' solution when $A = 0$. We solve (23)–(24) for initial data $u_n(0) = e^{-n^2}$ and $u_n'(0) = 0$. For zero Dirichlet boundary conditions the wave is reflected inside the computational domain, reaches its center and goes back to the boundary, giving rise to successive reflections. The nonreflecting conditions $u_t \pm u_x = 0$ for the wave equation $u_{tt} - u_{xx} = 0$ are discretized at each boundary as $u_{\pm N}^{j+1} - u_{\pm N}^j = h\sqrt{D}\left(-u_{\pm N}^j + u_{\pm(N-1)}^j\right)$, choosing $h$ and $\frac{1}{\sqrt{D}}$ as time step and spatial step respectively. Again, a wave of certain magnitude is reflected. The smaller $D$ becomes, the worse these conditions behave. Our nonreflecting boundary condition (20) discretized according to the scheme (23)–(25) suppresses the reflections for $\tau$ large. Our tests show that the spatial patterns agree with the 'exact' solution if $\tau \geqslant 10$. For small $\tau \leqslant 1$, a reflection at the boundary is observed, similar to the reflection generated with Dirichlet boundary conditions. Its magnitude diminishes as $\tau$ gets close to 1. For scattered ranges of intermediate $\tau \in (1, 10)$ a long time instability is detected. The evolution is initially stable. The outgoing waves of larger amplitude cross the boundary without departing from the true solution. Small amplitude oscillations about zero remain. Past a certain time (50–80 in our tests), the mean of the oscillations becomes positive and $u_n^j$ looks like a positive constant over the computational domain, which grows away from the true solution. We discuss the possible causes of this behavior in Section 3.4.

We compare the quality of the numerical solutions for different parameters by plotting reflexivity coefficients. Let $v_n^j$ be the exact solution in the small lattice and $u_n^j$ an approximate solution generated with artificial boundary conditions. We define the reflexivity coefficients $N(t)$ and $E(t)$ in terms of the euclidean norm of the difference and the relative error in the approximate energies:

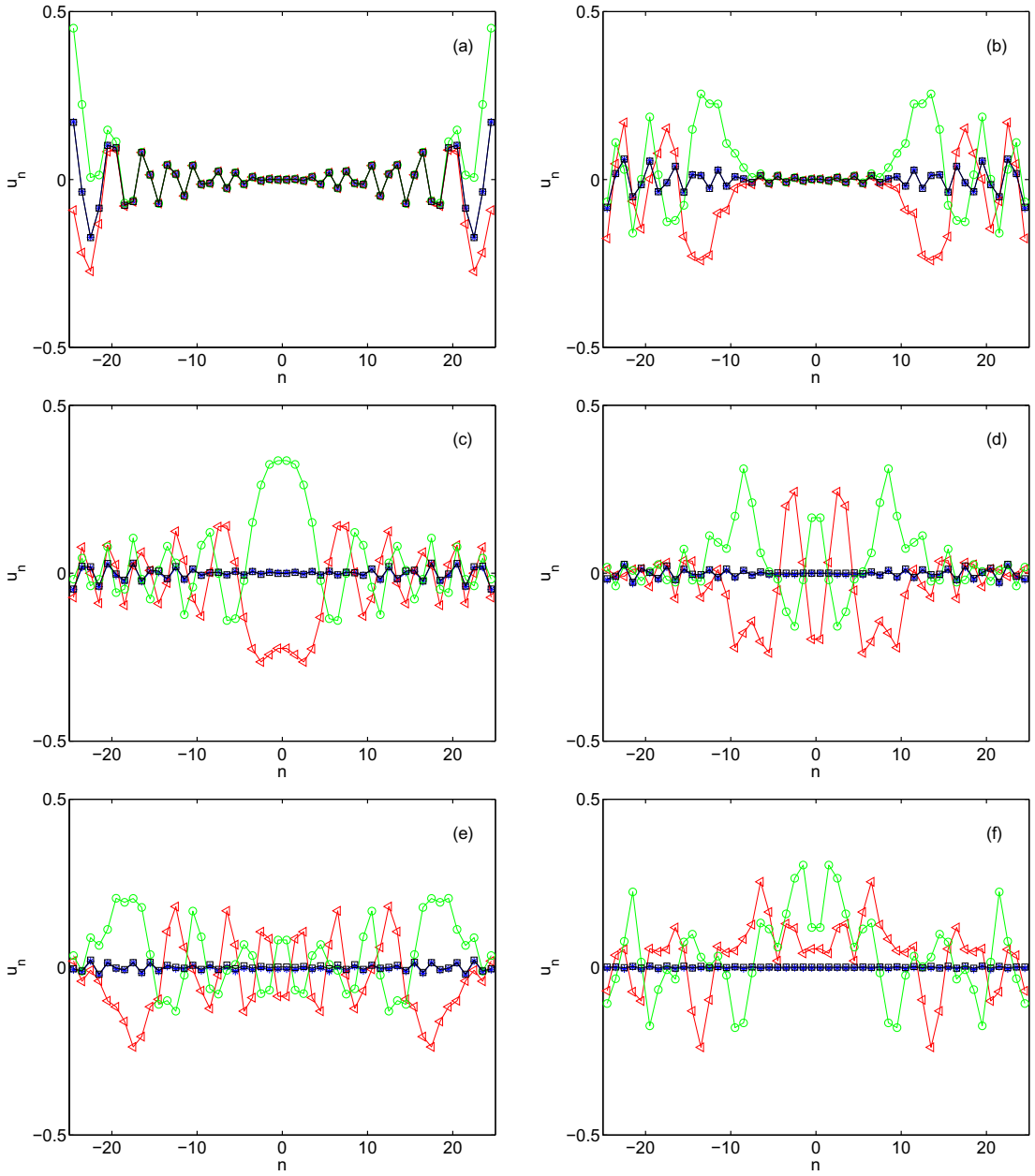


**Fig. 3.** Outgoing waves for $D = 1$, $A = 0$ at times (a) 27.20, (b) 38.70, (c) 50, (d) 60, (e) 70, (f) 200. Squares mark the true solution. Triangles correspond to zero Dirichlet boundary conditions, circles to discretized absorbing boundary conditions for wave equations and asterisks to (23)–(25). Parameter values are $\tau = 10, h = 10^{-2}, N_1 = 25, N_2 = 125$.

$$N(t_j) = \frac{\sqrt{\sum_{-N_1 \leqslant n \leqslant N_1} \left| u_n^j - v_n^j \right|^2}}{2N_1 + 1}, \tag{26}$$

$$E(t_j) = \frac{\left| \mathscr{E}\left(u_n^j\right) - \mathscr{E}\left(v_n^j\right) \right|}{\mathscr{E}\left(v_n^0\right)}, \quad \mathscr{E}\left(u_n^j\right) = \frac{1}{2} \sum_{-N_1 \leqslant n \leqslant N_1} \left| \frac{u_n^{j+1} - u_n^{j-1}}{2h} \right|^2 + \frac{D}{2} \sum_{-N_1 \leqslant n \leqslant N_1} \left| u_n^j - u_{n-1}^j \right|^2. \tag{27}$$

Fig. 4 plots these coefficients for (23)–(25) when $\tau = t$ (no truncation), $\tau = 50$ and $\tau = 10$. The magnitude of the reflections decreases as $\tau$ increases. Notice that $|K(t)| \leqslant 3 \times 10^{-2}$ when $t \geqslant 10$ and $|K(t)| \leqslant 3 \times 10^{-3}$ if $t \geqslant 50$. The smallest reflexivity coefficients are obtained when $t = \tau$. For $\tau = 10, 50$, the reflexivity coefficients are small but they increase as time grows.

Fig. 5 shows the evolution of the initial gaussian with $A = 1$ and $\tau = 50$. The spatial patterns are almost undistinguishable when $\tau = 50$ and $\tau = t$, for the time we have computed. As $\tau$ decreases, spurious small amplitude oscillations develop for large times. Reflexivity coefficients are plotted in Fig. 6. The appearance of spurious oscillations distorts Fig. 6(e) and (f)

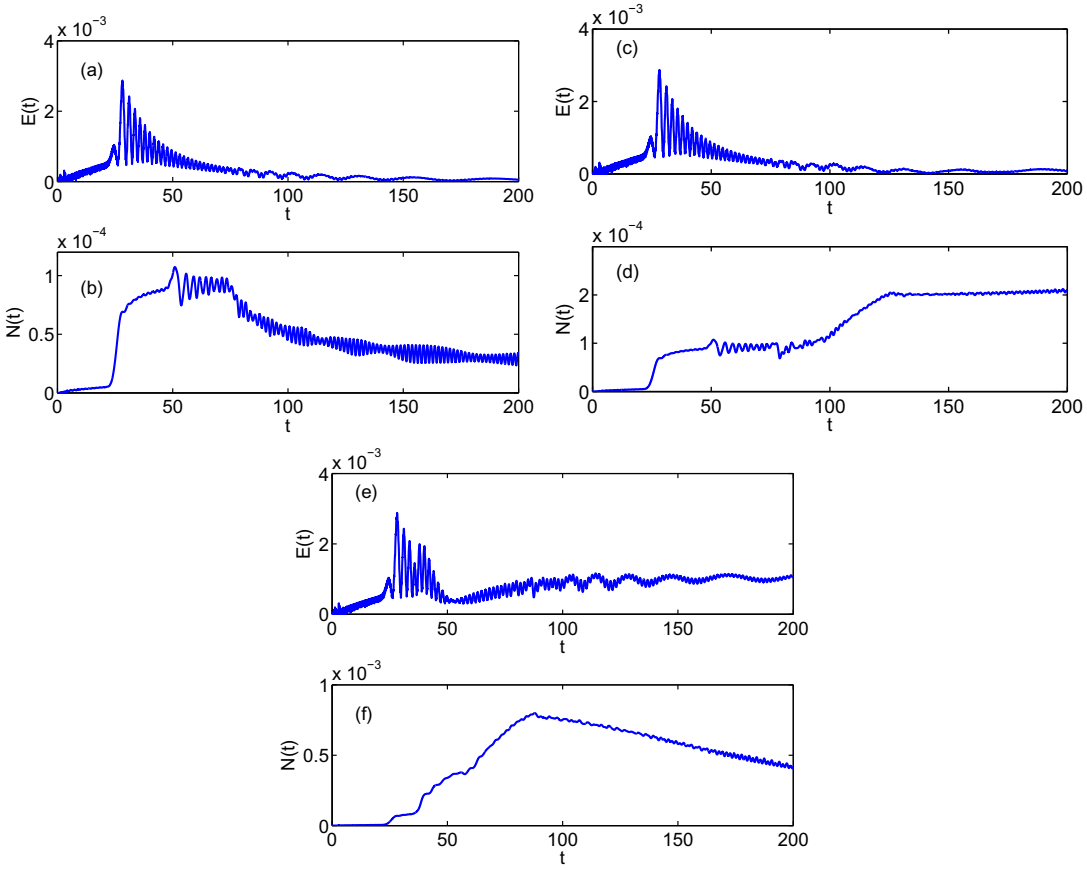


**Fig. 4.** Reflexivity coefficients for the second order scheme (23)–(25): (a) and (b) $\tau = t$, (c) and (d) $\tau = 50$, (e) and (f) $\tau = 10$. Parameter values are $D = 1, A = 0, h = 10^{-2}, N_1 = 25, N_2 = 125$.

for $\tau = 10$. Increasing $\tau$ delays and reduces this effect. No instabilities similar to the one encountered when $A = 0$ have been detected.

### 3.3. Higher order schemes

High order schemes allow to use larger time steps without amplifying the magnitude of the reflections or increase the precision without recalculating the weights $K(t_\ell)$. Let us write (2) as a first order system:

$$u_n' = v_n, \quad -N \leqslant n \leqslant N,\ t > 0, \tag{28}$$

$$v_n' = D(u_{n+1} - 2u_n + u_{n-1}) - Au_n = f(u_n), \tag{29}$$

with $u_{\pm(N+1)}$ defined in (21). We have designed a fourth order scheme combining a symplectic Runge–Kutta method of order four [36] to integrate (28) and (29):

$$g_1 = 0, \quad g_2 = 0.2052, \quad g_3 = 0.6082, \quad g_4 = 0.487, \quad g_5 = 1,$$
$$b_1 = 0.0617, \quad b_2 = 0.339, \quad b_3 = 0.6148, \quad b_4 = -0.1405, \quad b_5 = 0.125,$$
$$\beta_i = b_i(1 - g_i), \quad i = 1, \ldots, 5,$$
$$a_{i,j} = b_j(g_i - g_j), \quad i = 2, \ldots, 5, \quad j = 1, \ldots, i-1,$$
$$q_{1,n} = u_n^j + hg_1 v_n^j, \quad c_{1,n} = f(q_{1,n}),$$
$$q_{l,n} = u_n^j + hg_l v_n^j + h^2 \sum_{i=1}^{l-1} a_{l,i} c_{i,n}, \quad c_{l,n} = f(q_{l,n}), \quad l = 2, \ldots, 5,$$
$$u_n^{j+1} = u_n^j + hv_n^j + h^2 \sum_{i=1}^{5} \beta_i c_{i,n}, \quad v_n^{j+1} = v_n^j + h \sum_{i=1}^{5} b_i c_{i,n},$$

and the quadrature formula (25), with the coefficients of the composite Simpson rule $c_0 = \frac{1}{3}$, $c_{2j-1} = \frac{4}{3}$, $c_{2j} = \frac{2}{3}$, $j = 1, \ldots, n_\tau - 1$, $c_{n_\tau} = \frac{1}{3}$, to compute the integrals in (21). As Figs. 7 and 4 show, the quality of the solutions generated by the fourth and second order schemes when $h = 10^{-1}$ and $h = 10^{-2}$, respectively, is similar. The magnitude of the truncation error is also

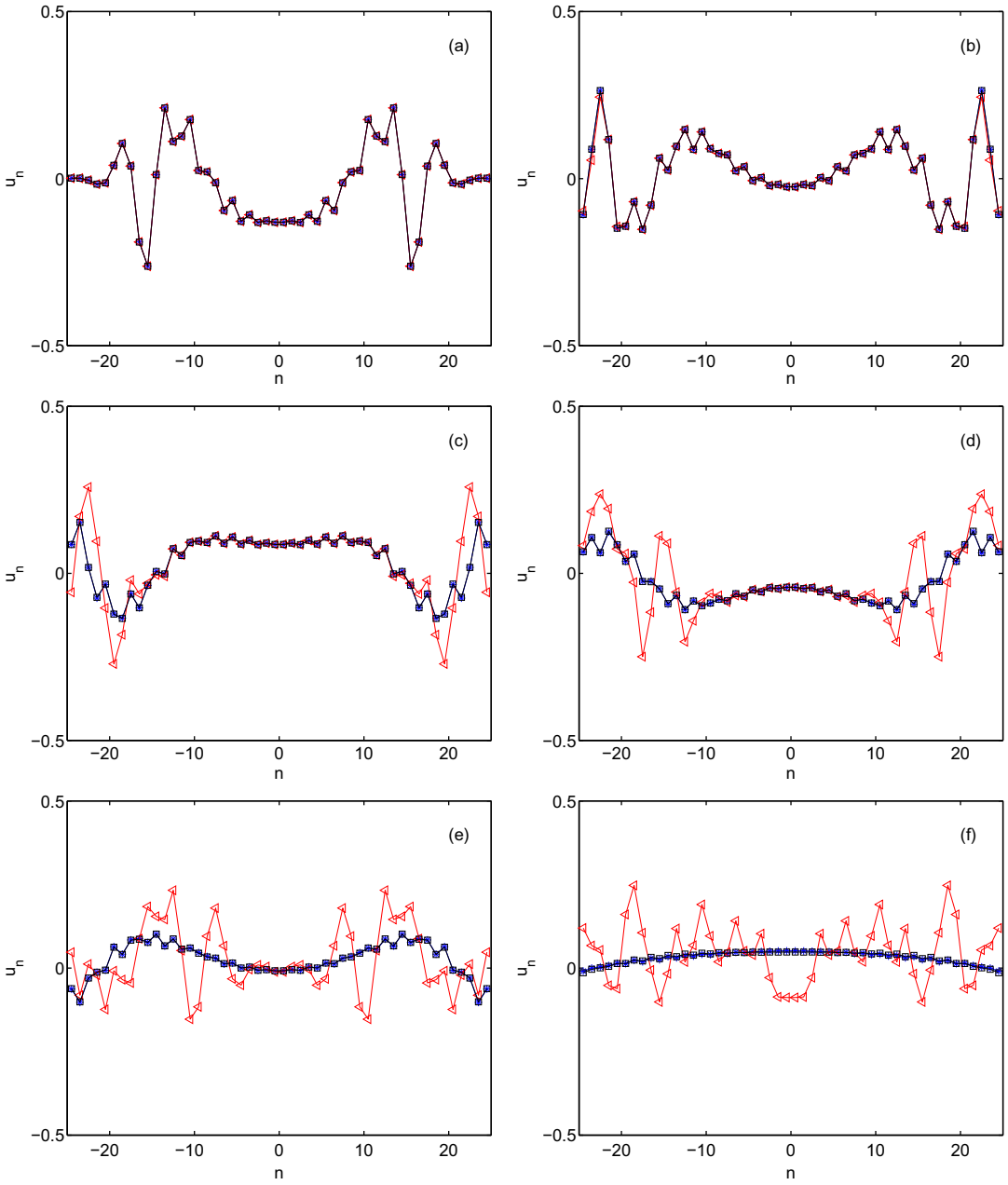


**Fig. 5.** Outgoing waves for $D = 1, A = 1$ at times (a) 27.20, (b) 38.70, (c) 50, (d) 60, (e) 70, (f) 200. Squares mark the true solution. Triangles correspond to zero Dirichlet boundary conditions and asterisks to (23)–(25). Parameter values are $\tau = 50, h = 10^{-2}, N_1 = 25, N_2 = 100$.

expected to be similar. However, less steps mean less convolutions to be computed, reducing the cost. Long time instabilities persist when $A = 0$, for the same values of $\tau$ for which they are detected in Section 3.2.

### 3.4. Long time instability

A possible explanation for the detected instability is the following. When $A = 0$, the discrete wave Eq. (2) has solutions of the form $u_n(t) = \varepsilon t$, satisfying $u_n(0) = 0$ and $u_n'(0) = \varepsilon$. The equivalent problem set in $|n| \leqslant N$ with integrodifferential boundary conditions (20) and (21) has the same solutions. If we truncate the integral in (20) to the interval $[t - \tau, t]$, the resulting problem should also have unbounded solutions for $\tau$ large. Tracking numerically the evolution of $u_n(0) = 0$ and $u_n'(0) = \varepsilon$ for the scheme (23)–(25), the corresponding solutions seem to remain bounded for small $\tau \leqslant \tau_0$, but grow unboundedly if $\tau > \tau_0$ and $\varepsilon \geqslant \varepsilon(\tau)$. In $(\tau_0, \tau_1)$, the oscillatory behavior of $K$ selects alternate ranges of $\tau$ for which $\varepsilon(\tau)$ is smaller. The values of $\tau$ for which we have detected long time instabilities in our simulations seem to fall in these ranges. Notice that the solutions generated in Section 3.2 become almost zero at a time $T$. The solution and its derivative are close to both $u_n(T) = 0, u_n'(T) = 0$ and $u_n(T) = 0$, $u_n'(T) = \varepsilon, \varepsilon$ small. Therefore, as time grows, it may be attracted by zero or by an unbounded attractor. For some ranges of intermediate $\tau \in (\tau_0, \tau_1), \varepsilon(\tau)$ is small enough and the long time reflections are large

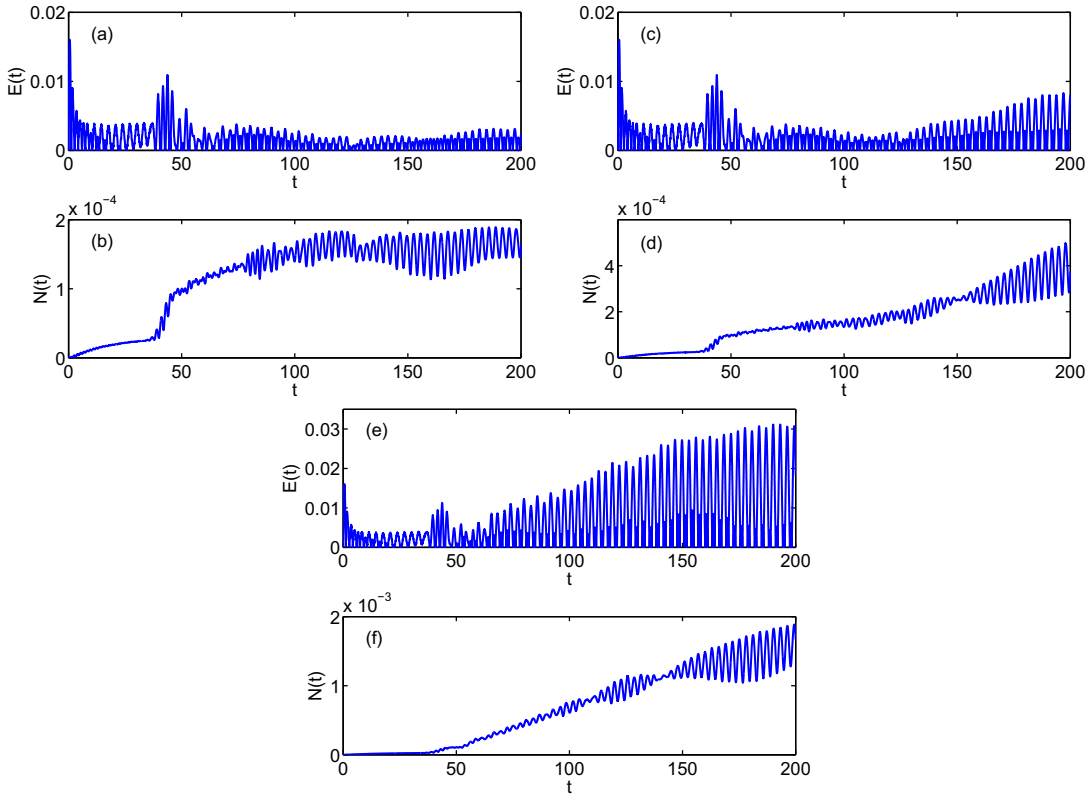


**Fig. 6.** Reflexivity coefficients for the second order scheme (23)–(25): (a) and (b) $\tau = t$, (c) and (d) $\tau = 50$, (e) and (f) $\tau = 10$. Parameter values are $D = 1, A = 1, h = 10^{-2}, N_1 = 25, N_2 = 100$.

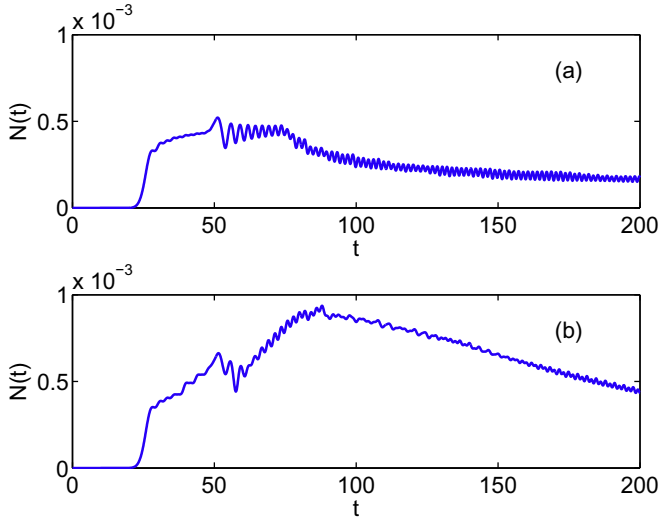


**Fig. 7.** Reflexivity coefficients for the fourth order scheme with (a) $\tau = t$ and (b) $\tau = 10$. Parameter values are $D = 1, A = 0, h = 10^{-1}, N_1 = 25$ and $N_2 = 125$.

enough for the truncation error to drive the solution away from zero. When $\tau \geqslant \tau_1$, the truncation error remains small enough to avoid this. Note that (2) does not admit solutions of the form $u_n(t) = \varepsilon t$ when $A \neq 0$.

## 4. Extension to higher dimensions

Let us consider a simple cubic crystal lattice. We label its atoms using three integer parameters $\mathbf{n} = (n_1, n_2, n_3)$. The displacement of each atom from its equilibrium position is $\mathbf{u} = (\mathbf{u_n})$. We denote the crystal energy by $U(\mathbf{u})$. The nonlinear dimensionless equations of motion are:

$$M\frac{d^2\mathbf{u_n}}{dt^2} = -\frac{\partial U(\mathbf{u})}{\partial \mathbf{u_n}}. \tag{30}$$

Here, $\mathbf{u_n}$ is the dimensionless displacement vector of the atom labeled as $\mathbf{n}$. $M$ is its dimensionless mass. Often, $U(\mathbf{u}) = \frac{1}{2}\sum_{\mathbf{n}'\neq\mathbf{n}} V(|\mathbf{u_{n'}} - \mathbf{u_n}|)$, for some interatomic potential $V$. If all crystal defects are concentrated in a small region, at a certain distance the equations of motion may be linearized and localized. Using nearest neighbor interactions, the vectorial equations of motion are:

$$M\frac{d^2\mathbf{u_n}}{dt^2} = \sum_{|n_1-n_1'|\leqslant 1, |n_2-n_2'|\leqslant 1, |n_3-n_3'|\leqslant 1} \mathbf{C_{n-n'}}\mathbf{u_{n'}} \tag{31}$$

with dimensionless coefficient matrices $\mathbf{C_{n-n'}}$ related to the elastic constants of the lattice: $\mathbf{C_{n-n'}} = -\frac{\partial^2 U(\mathbf{u})}{\partial \mathbf{u_{n'}}\partial \mathbf{u_n}}\Big|_{\mathbf{u}=0}$.

### 4.1. A spatially discrete wave equation

For a discrete wave equation the matrices $\mathbf{C_{n-n'}}$ are particularly simple:

$$\frac{d^2\mathbf{u_n}}{dt^2} = D\sum_{|\mathbf{n}-\mathbf{n}'|\leqslant 1} (\mathbf{u_{n'}} - \mathbf{u_n}) \tag{32}$$

with $D > 0, \mathbf{n} = (n_1, n_2, n_3)$ and $\mathbf{n}' = (n_1', n_2', n_3')$. The system uncouples and we can work component-wise. We truncate the computational domain to a finite box, placing artificial boundaries at $\{|n_1| = N_1, |n_2| = N_2, |n_3| = N_3\}$, and look for a nonreflecting boundary condition. Again, the first step is to compute the Green's function for the initial value problem in the whole space.

#### 4.1.1. Green's functions

We wish to find an integral expression for the solution of:

$$\frac{d^2 u_{\mathbf{n}}}{dt^2} = D\sum_{|\mathbf{n}-\mathbf{n}'|\leqslant 1} (u_{\mathbf{n}'} - u_{\mathbf{n}}) + f_{\mathbf{n}}, \tag{33}$$

$$u_{\mathbf{n}}(0) = u_{\mathbf{n}}^0, \quad \frac{du_{\mathbf{n}}}{dt}(0) = u_{\mathbf{n}}^1. \tag{34}$$

The associated Green's functions can be found following the strategy described in Section 2.1: remove the difference operator using discrete Fourier transforms

$$p(\theta, t) = \sum_{\mathbf{n}} u_{\mathbf{n}}(t)e^{-i\mathbf{n}\cdot\theta}, \quad f(\theta, t) = \sum_{\mathbf{n}} f_{\mathbf{n}}(t)e^{-i\mathbf{n}\cdot\theta}, \quad \theta = (\theta_1, \theta_2, \theta_3). \tag{35}$$

Differentiating $p$ with respect to $t$, (33) implies that $p$ solves (6) with $\omega(\theta)^2 = 4D\left[\sin^2\left(\frac{\theta_1}{2}\right) + \sin^2\left(\frac{\theta_2}{2}\right) + \sin^2\left(\frac{\theta_3}{2}\right)\right]$. The initial conditions for $p$ follow from the initial conditions for $u_{\mathbf{n}}$. Again, $p$ depends on the roots of $r^2 + \omega(\theta)^2 = 0$ and is given by (7). We recover $u_{\mathbf{n}}$ inverting the Fourier transforms to get (9). Now, $\mathbf{n}$, $\mathbf{k}$ and $\theta$ are vectors and the Green's functions are given by:

$$G_{\mathbf{n},\mathbf{k}}(t) = \int_{-\pi}^{\pi}\int_{-\pi}^{\pi}\int_{-\pi}^{\pi} \frac{d\theta}{(2\pi)^3}\frac{e^{i(\mathbf{n}-\mathbf{k})\cdot\theta}}{\omega(\theta)}\sin(\omega(\theta)t). \tag{36}$$

Discrete Klein–Gordon equations can be handled modifying the expression for $\omega$: $\omega(\theta)^2 = 4D\left[\sin^2\left(\frac{\theta_1}{2}\right) + \sin^2\left(\frac{\theta_2}{2}\right) + \sin^2\left(\frac{\theta_3}{2}\right)\right] + A, A > 0$, as done in Section 2. Once the Green's functions for the initial value problem are known, we may construct nonreflecting boundary conditions for a half-space.

#### 4.1.2. Exact nonreflecting boundary conditions for a half-space

Let us place an artificial boundary at $n_1 = 0$ and try to solve (33) for $n_1 \geqslant 0$. A boundary condition to compute $u_{0,\mathbf{m}}(t), \mathbf{m} = (n_2, n_3)$ is needed. At the wall $n_1 = 0$, (33) reduces to:

$$\frac{d^2 u_{0,\mathbf{m}}}{dt^2} = D\sum_{|n_1'|+|\mathbf{m}-\mathbf{m}'|\leqslant 1} (u_{n_1',\mathbf{m}'} - u_{0,\mathbf{m}}) + f_{0,\mathbf{m}}, \tag{37}$$

with $\mathbf{m}' = (n_2', n_3')$. These equations involve the unknown values $u_{-1,\mathbf{m}}$. We must express them in terms of the values in the half-space $n_1 \geqslant 0$ to close the system. As in Section 2, we can find a formula for them assuming we know $u_{0,\mathbf{m}}$ for all $\mathbf{m}$ and solving (33)–(34) in the half-space $n_1 \leqslant 0$, with $u_{0,\mathbf{m}}$ as boundary data. This problem can be rewritten with homogeneous boundary conditions incorporating the boundary condition in a modified source term $f_{n_1,\mathbf{m}} + \delta_{n_1,-1}Du_{0,\mathbf{m}}$. Notice that Eq. (33) for $u_{-1,\mathbf{m}}$ involves only the points $u_{-2,\mathbf{m}}, u_{0,\mathbf{m}}$ and $u_{-1,\mathbf{m}'}, |\mathbf{m} - \mathbf{m}'| \leqslant 1$. This allows for an odd extension

$$v_{n_1,\mathbf{m}} = \begin{cases} u_{n_1,\mathbf{m}} & n_1 < 0 \\ 0 & n_1 = 0 \\ -u_{-n_1,\mathbf{m}} & n_1 > 0, \end{cases} \tag{38}$$

which solves a problem set in the whole space:

$$\frac{d^2 v_{n_1,\mathbf{m}}}{dt^2} = D \sum_{|n_1-n_1'|+|\mathbf{m}-\mathbf{m}'|\leqslant 1} (v_{n_1',\mathbf{m}'} - v_{n_1,\mathbf{m}}) + g_{n_1,\mathbf{m}}, \tag{39}$$

$$v_{n_1,\mathbf{m}}(0) = v^0_{n_1,\mathbf{m}}, \quad \frac{dv_{n_1,\mathbf{m}}}{dt}(0) = v^1_{n_1,\mathbf{m}}. \tag{40}$$

The initial data $v^0_{n_1,\mathbf{m}}$ and $v^1_{n_1,\mathbf{m}}$ are odd extensions of $u^0_{n_1,\mathbf{m}}$ and $u^1_{n_1,\mathbf{m}}$ defined as in (38). The source $g_{n_1,\mathbf{m}}$ is constructed with a similar odd extension of $g_{n_1,\mathbf{m}} = f_{n_1,\mathbf{m}} + D\delta_{n_1,-1}u_{0,\mathbf{m}}$, $n_1 < 0$, to positive $n_1$ (see (15) and (56)). Expressing $v_{n_1,\mathbf{m}}$ in terms of Green's functions as in Section 4.1.1 and exploiting the symmetry of the data, we find an expression for $u_{-1,\mathbf{m}}$:

$$u_{-1,\mathbf{m}}(t) = r_{-1,\mathbf{m}}(t) + D \sum_{\mathbf{m}'\in\mathbb{Z}^2} \int_0^t \mathscr{G}_{(-1,\mathbf{m}),(-1,\mathbf{m}')}(t-s)u_{0,\mathbf{m}'}(s)ds, \tag{41}$$

$$r_{-1,\mathbf{m}}(t) = \sum_{n_1'<0,\mathbf{m}'\in\mathbb{Z}^2} \left[ \mathscr{G}_{(-1,\mathbf{m}),(n_1',\mathbf{m}')}(t)\frac{du_{n_1',\mathbf{m}'}}{dt}(0) + \frac{d\mathscr{G}_{(-1,\mathbf{m}),(n_1',\mathbf{m}')}}{dt}(t)u_{n_1',\mathbf{m}'}(0) + \int_0^t \mathscr{G}_{(-1,\mathbf{m}),(n_1',\mathbf{m}')}(t-s)f_{n_1',\mathbf{m}'}(s)ds \right], \tag{42}$$

where $\mathscr{G}_{(n_1,\mathbf{m}),(n_1',\mathbf{m}')} = G_{(n_1,\mathbf{m}),(n_1',\mathbf{m}')} - G_{(n_1,\mathbf{m}),(-n_1',\mathbf{m}')}$ is the Green's function for the half-space $n_1 < 0$ with zero boundary condition $n_1 = 0$. The source term $r_{-1,\mathbf{m}}(t)$ represents the contribution of the data in the outer region and its impact on the dynamics inside the truncated computational domain.

The boundary condition at the wall $n_1 = 0$ is given by (37) and (41). Boundary conditions for other planes are computed in a similar way. Conditions (37) and (41) apply in 2D replacing $\mathbf{m} = (n_2, n_3)$ by $m = n_2$.

### 4.1.3. Approximate boundary conditions in a finite box

Once the nonreflecting boundary condition for a half-space is known, we may obtain approximate boundary conditions for boxes. Let $n_1 = \pm N_1, n_2 = \pm N_2$ and $n_3 = \pm N_3$ be the walls of a 3D cubic box. On each wall, we impose a truncated nonreflecting boundary condition for the corresponding half-space. The infinite sum in (41) can be approximated by a finite sum using the decay of $\mathscr{G}_{(-1,\mathbf{m}),(-1,\mathbf{m}')}(t)$ as $|\mathbf{m}-\mathbf{m}'|$ grows. We only keep the terms for which $|\mathbf{m}-\mathbf{m}'| \leqslant M$. The integral over $[0,t]$ can also be approximated by an integral over $[t-\tau, t]$, choosing $\tau \geqslant 0$ large enough. If we want to use this type of boundary conditions on the walls $n_1 = \pm N_1$ of the box, (41) becomes:

$$u_{\pm(N_1+1),\mathbf{m}}(t) = r_{\pm(N_1+1),\mathbf{m}}(t) + D\sum_{\mathbf{m}'\in\mathbf{I}} \int_{(t-\tau)^+}^t \mathscr{G}_{(-1,\mathbf{m}),(-1,\mathbf{m}')}(t-s)u_{\pm N_1,\mathbf{m}'}(s)ds, \tag{43}$$

where $\mathbf{I} = \{(n_2', n_3') \,|\, |n_2'| \leqslant N_2, |n_3'| \leqslant N_3, |n_2 - n_2'| \leqslant M, |n_3 - n_3'| \leqslant M\}$. These conditions cease to be exact because of the truncation error, which is larger at the edges and the corners.

The same strategy can be adopted for 2D cubic lattices. The approximate boundary conditions on the walls $n_1 = \pm N_1$ are then:

$$\frac{d^2 u_{\pm N_1,n_2}}{dt^2} = D \sum_{|\pm N_1 - n_1'|+|n_2-n_2'|\leqslant 1} (u_{n_1',n_2'} - u_{\pm N_1,n_2}) + f_{\pm N_1,n_2}, \tag{44}$$

$$u_{\pm(N_1+1),n_2}(t) = r_{\pm(N_1+1),n_2}(t) + D\sum_{n_2'\in\mathbf{I}} \int_{(t-\tau)^+}^t K^{\pm}_{n_2-n_2'}(t-s)u_{\pm N_1,n_2'}(s)ds, \tag{45}$$

$$r_{\pm(N_1+1),n_2}(t) = \sum_{\mathbf{m}'\in\mathbf{R}} \left[ K^{\pm}_{n_1',n_2-n_2'}(t)\frac{du_{n_1',n_2'}}{dt}(0) + \frac{dK^{\pm}_{n_1',n_2-n_2'}}{dt}(t)u_{n_1',n_2'}(0) + \int_{(t-\tau)^+}^t K^{\pm}_{n_1',n_2-n_2'}(t-s)f_{n_1',n_2'}(s)ds \right], \tag{46}$$

where

$$\mathbf{I} = \{n_2' \,|\, |n_2'| \leqslant N_2, |n_2 - n_2'| \leqslant M\},$$
$$\mathbf{R} = \{(n_1', n_2') \,|\, (N_1 \mp n_1') < 0, |n_2 - n_2'| \leqslant M, |\pm 1 + (n_1' \pm N_1)| \leqslant M\},$$
$$K^{\pm}_{n_1',n_2-n_2'} = \mathscr{G}_{(\pm 1,n_2),(-(n_1'\pm N_1),n_2')}, \; K^{\pm}_{n_2-n_2'} = \mathscr{G}_{(\pm 1,n_2),(\pm 1,n_2')},$$
$$\mathscr{G}_{(n_1,n_2),(n_1',n_2')} = G_{(n_1,n_2),(n_1',n_2')} - G_{(n_1,n_2),(-n_1',n_2')},$$

and $G_{\mathbf{n},\mathbf{n}'}(t)$ is the two dimensional version of (36). The boundary conditions on the walls $n_2 = \pm N_1$ are similar, interchanging the roles of the first and second subscripts and replacing $n_2, n_2'$ with $n_1, n_1'$.

### 4.1.4. Numerical scheme

We have used these boundary conditions to simulate the evolution of a gaussian in a 2D cubic square lattice with the dynamics (32). Conditions (44) and (45) apply on the artificial boundaries $n_1 = \pm N$ with $r_{\pm(N+1)} = 0$. Equivalent formulas

(interchanging the roles of $n_1$ and $n_2$) are imposed on the artificial boundaries $n_2 = \pm N$. The kernels $K^{\pm}_{n_2-n_2'}(t)$, defined by the expressions

$$K^{\pm}_{n_2-n_2'}(t) = \int_{-\pi}^{\pi}\int_{-\pi}^{\pi} \frac{d\theta_1 d\theta_2}{(2\pi)^2} \frac{(1-e^{\pm i2\theta_1})e^{i(n_2-n_2')\theta_2}}{\omega(\theta)} \sin(\omega(\theta)t), \tag{47}$$

are evaluated at the grid points $t_\ell = \ell h, 0 \leqslant l \leqslant L, Lh = T$, and stored from the start. They are computed using adaptive Lobatto quadrature with tolerance $10^{-6}$. By symmetry, the kernels for the walls $n_1 = N$ and $n_2 = N$ or $n_1 = -N$ and $n_2 = -N$ agree.

We discretize (32) using the second order scheme described in Section 3, generalized to two dimensions. Time derivatives are discretized using (22). The time integrals in (44) and (45) are truncated to intervals $[t-\tau, t]$, $\tau \geqslant 0$, and approximated by composite trapezoidal rules. Alternatively, we might proceed as in Section 3.3 to reduce the number of time steps. At each time step we have to evaluate $8N$ discrete convolutions of the form $\sum_{\ell=0}^{n_\tau} g(t_\ell)w(t_j - t_\ell)$, with $g(0) = 0, n_\tau h = \tau$. Reasonable results are obtained for small values of $N, \tau$ and $M$ without turning to acceleration techniques. For large lattices or cut-off values $\tau$ and $M$, we may resort to fast Fourier transforms or parallelize the evaluation of convolutions to speed up the process.

Nonreflecting boundary conditions for wave equations usually give rise to discrete convolutions where the Laplace transform of $g(t)$ is known and has a simple explicit form. Specific acceleration techniques to evaluate such sums are discussed in [32]. It is unclear whether similar strategies might be applied with success in our case. We do not need to compute convolutions with a large or increasing number of terms because we exploit the time decay of our kernels to truncate the time integrals over $[0, t]$ to integrals over intervals of fixed length $\tau$. Also, we do not have simple explicit forms for the Laplace transforms of the kernels. We evaluate the kernels directly from the start.

#### 4.1.5. Numerical results

To calibrate reasonable choices of the cut-off parameters $\tau$ and $M$ in (45) we first simulate the evolution of an initial gaussian in a half-space. The left wall is located at $N = -10$. Fig. 8 plots the reflexivity coefficient

$$N(t_j) = \frac{\sqrt{\sum_{-N\leqslant n_1,n_2\leqslant N}\left|u^j_{n_1,n_2} - v^j_{n_1,n_2}\right|^2}}{(2N+1)^2}, \tag{48}$$

for different $M$ and $\tau$. $u^j_{n_1,n_2}$ is generated using data $u^0_{n_1,n_2} = e^{-n_1^2-n_2^2}, u^1_{n_1,n_2} = 0$ in a truncated domain and $v^j_{n_1,n_2}$ is the reference 'exact' solution. For each choice of $\tau$, there is a threshold value of $M$ above which no improvement is to be expected. This threshold is about 1 for $\tau = 1, 5$ for $\tau = 5\ldots$ Similarly, for each fixed $M$, the reflexivity coefficients agree if $\tau$ is large enough. This happens if $\tau$ is larger than $5, 10, 10, 20\ldots$ for $M = 1, 2, 5, 10\ldots$, respectively. For each $M$, there seems to be a critical value of $\tau$ above which the reflexivity coefficient does not improve and may even worsen. The best reflexivity coefficients for $M = 5, 10$, seem to correspond to $\tau = 5, 10$, respectively.

The reflexivity coefficients allow to compare the magnitude of the reflexions for different $\tau$ and $M$. To check the quality of the solutions, we visualize the time evolution of the spatial patterns. Fig. 9 represents the evolution of the wave when $\tau = 5$, for decreasing $M$. Snapshots (g)–(h) show a small reflected wave when $M = 1$. If $M = 2$, this reflected wave persists, see

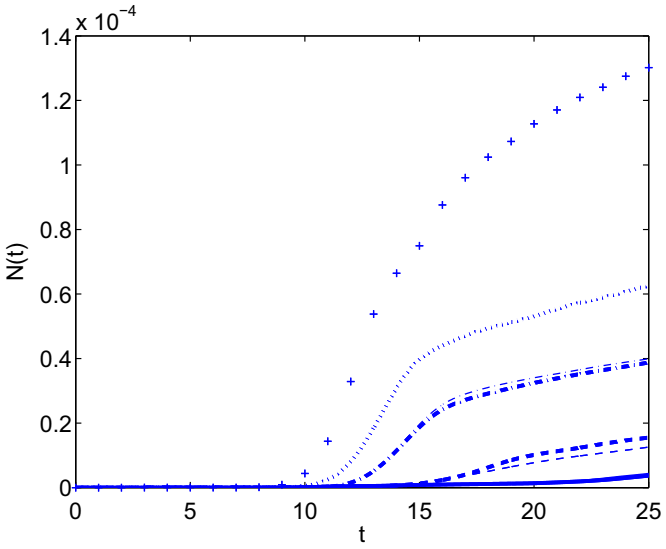


**Fig. 8.** Reflexivity coefficients for half-spaces. Thick lines correspond to $\tau = 10$ for different values of the cut-off value $M$: $M = 10$ (solid), $M = 5$ (dashed), $M = 2$ (dash-dotted) and $M = 1$ (dotted). Thin lines correspond to $\tau = 5$ for $M = 5$ and $M = 2$. Crosses mark the reflexivity coefficient when $M = 1$ and $\tau = 1$. Other parameter values are $h = 10^{-2}$ and $D = 1$.

Fig. 9(e)–(f). When $M = 5$, no reflected wave is seen in Fig. 9(a)–(d). $N(t)$ is of order $10^{-5}$. This set of parameters is acceptable because no reflected waves are appreciated at first sight. When $M = 2$ or $M = 1, N(t)$ has orders $4 \times 10^{-5}$ and $6 \times 10^{-5}$, respectively. Decreasing $\tau$, the magnitude of the reflected wave increases, until it becomes similar to the one generated with zero Dirichlet boundary conditions (see Fig. 2(g)–(h)) and $N(t)$ is of order $10^{-3}$.

The test in the half-space suggests the choice $M = 5$ and $\tau = 5$ for square lattices. Fig. 2(a)–(f) shows the evolution of the gaussian with walls located at $n_1 = \pm 10$ and $n_2 = \pm 10$. It is almost undistinguishable from the true solution, especially while the larger waves are exiting the lattice. Once the relevant fronts have left, the remaining small oscillations are affected by errors at the corners. The patterns do not worsen significantly by lowering $M$ to 2 or 1, and the cost is much smaller. Fig. 10 shows that for a given lattice size, the reflections cannot be reduced below some level (which decreases as the size

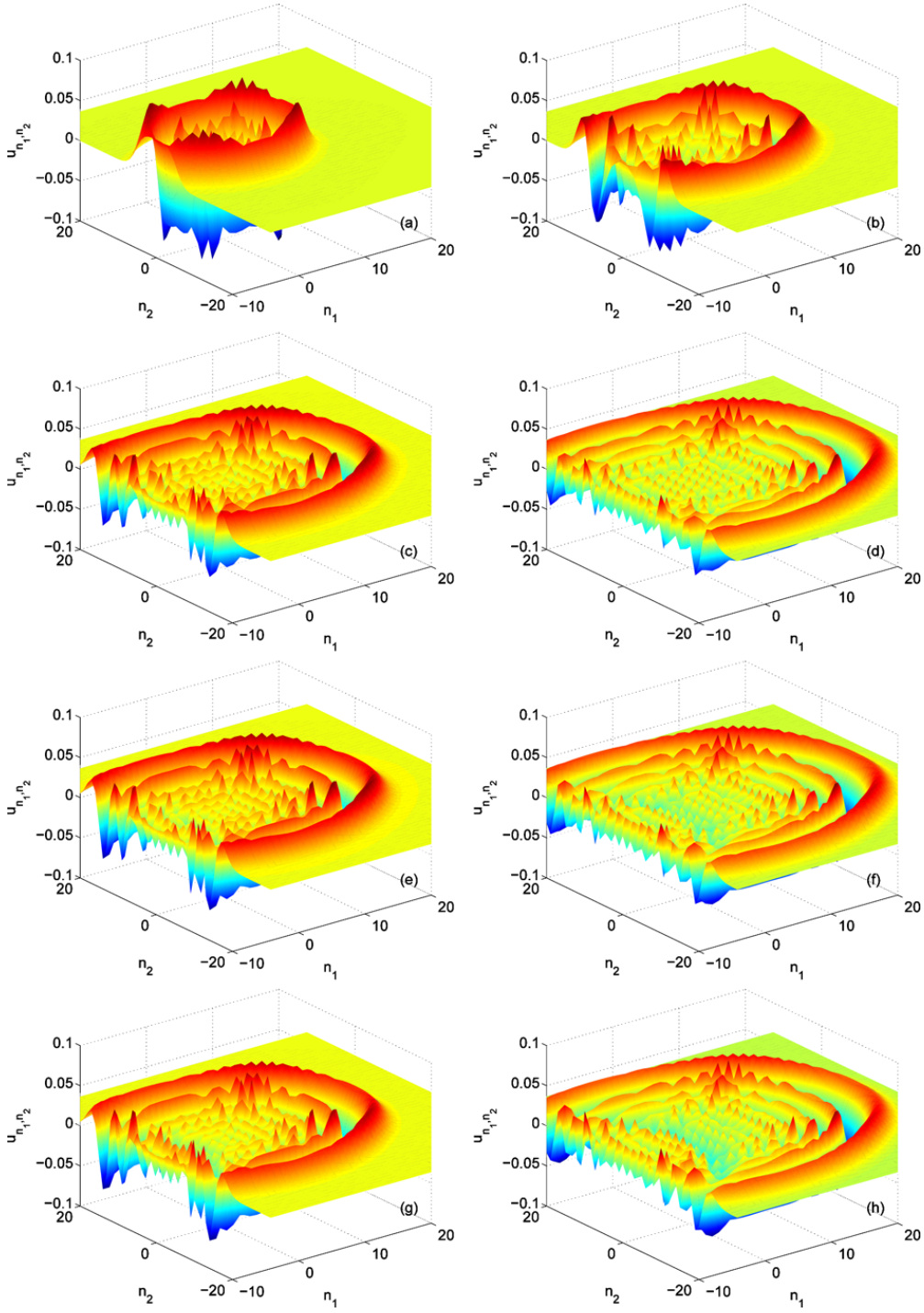


**Fig. 9.** Outgoing wave in a half-space limited by a wall placed at $n_1 = -10$, computed using (44)–(45) and decreasing $M$: (a) $M = 5, t = 10$, (b) $M = 5, t = 15$, (c) $M = 5, t = 20$, (d) $M = 5, t = 25$, (e) $M = 2, t = 20$, (f) $M = 2, t = 25$, (g) $M = 1, t = 20$, (h) $M = 1, t = 25$. Other parameter values are $h = 10^{-2}, \tau = 5, D = 1$.

of the lattice increases) by varying $\tau$ and $M$ due to the corners. Notice that $N(t)$ increases by a factor 10 compared to Fig. 8. Unlike the one dimensional case, we have detected no instabilities in our tests.

### 4.2. General case

To solve (31) we truncate the computational domain to a box, placing artificial boundaries at $|n_1| = N_1, |n_2| = N_2, |n_3| = N_3$, as in the previous section. Let us first compute the Green's function of the infinite initial value problem.

#### 4.2.1. Green's functions

To compute the Green's functions of the linearized operator (31) we follow Section 4.1.1. Let us consider the initial value problem

$$M\frac{d^2\mathbf{u}_\mathbf{n}}{dt^2} = \sum_{|n_1-n_1'|\leqslant 1, |n_2-n_2'|\leqslant 1, |n_3-n_3'|\leqslant 1} \mathbf{C}_{\mathbf{n}-\mathbf{n}'}\mathbf{u}_{\mathbf{n}'} + \mathbf{f}_\mathbf{n}, \tag{49}$$

$$\mathbf{u}_\mathbf{n}(0) = \mathbf{u}_\mathbf{n}^0, \quad \mathbf{u}_\mathbf{n}'(0) = \mathbf{u}_\mathbf{n}^1. \tag{50}$$

Now, $\mathbf{f}_\mathbf{n}$ and $\mathbf{u}_\mathbf{n}$ are vectors and $\mathbf{C}_\mathbf{n}$ matrices. The discrete transform $\mathbf{p}$ solves

$$M\frac{d^2\mathbf{p}}{dt^2}(\theta,t) + \mathbf{A}(\theta)\mathbf{p}(\theta,t) = \mathbf{f}(\theta,t), \quad \mathbf{A}(\theta) = \sum_{|n_1|\leqslant 1, |n_2|\leqslant 1, |n_3|\leqslant 1} \mathbf{C}_\mathbf{n} e^{-i\theta\cdot\mathbf{n}}. \tag{51}$$

Notice that the coefficient matrix $\mathbf{A}(\theta)$ does not depend on time. To find the general solution, we take the Laplace transform in time:

$$L\mathbf{p}(\theta,s) = (Ms^2\mathbf{I} - \mathbf{A}(\theta))^{-1}(L\mathbf{f}(\theta,s) + M\frac{d\mathbf{p}}{dt}(\theta,0) + sM\mathbf{p}(\theta,0)). \tag{52}$$

Setting $L\mathbf{G}_0(s) = (Ms^2\mathbf{I} - \mathbf{A}(\theta))^{-1}, L\mathbf{G}_1(s) = s(Ms^2\mathbf{I} - \mathbf{A}(\theta))^{-1} = L\mathbf{G}_0'(s)$, and inverting the Laplace transform, we find

$$\mathbf{p}(\theta,t) = M\frac{d\mathbf{G}_0}{dt}(t)\mathbf{p}(\theta,0) + M\mathbf{G}_0(t)\frac{d\mathbf{p}}{dt}(\theta,0) + \int_0^t \mathbf{G}_0(t-s)\mathbf{f}(\theta,s)ds. \tag{53}$$

Inverting the discrete Fourier transform we get (9) with:

$$\mathbf{G}_{\mathbf{n},\mathbf{k}}(t) = \int_{-\pi}^{\pi}\int_{-\pi}^{\pi}\int_{-\pi}^{\pi}\frac{d\theta}{(2\pi)^3}e^{i(\mathbf{n}-\mathbf{k})\cdot\theta}\mathbf{G}_0(s)ds. \tag{54}$$

#### 4.2.2. Exact nonreflecting boundary conditions for a half-space

Once we know the Green's function, a boundary condition for a half-space is obtained following Section 4.1.2, with small adjustments. We locate an artificial boundary at $n_1 = 0$. To solve (31) when $n_1 \geqslant 0$, a boundary condition is needed for $u_{0,\mathbf{m}}(t), \mathbf{m} = (n_2, n_3)$. On the wall $n_1 = 0$

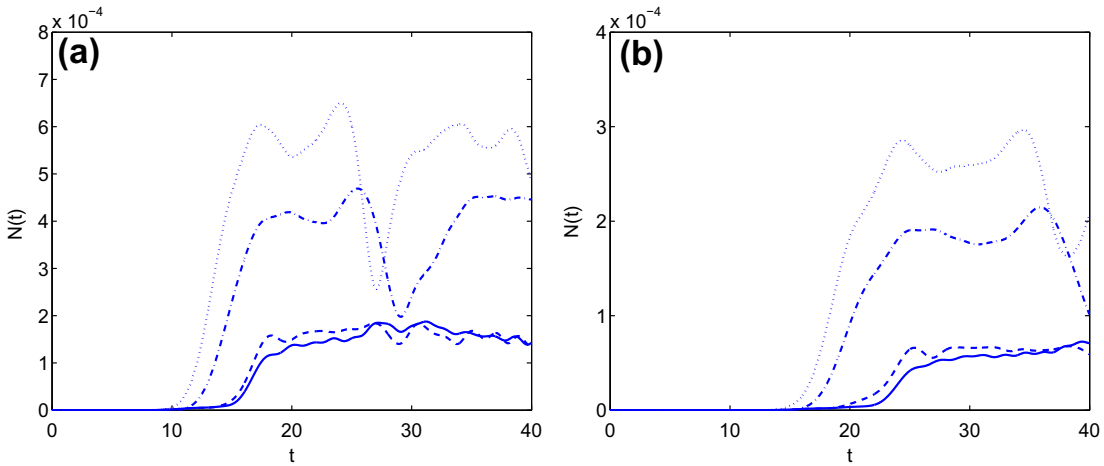


**Fig. 10.** Reflexivity coefficients for the tests in square lattices with walls located at (a) $N_1 = \pm 10, N_2 = \pm 10$ and (b) $N_1 = \pm 15, N_2 = \pm 15$. The curves correspond to $M = 10, \tau = 10$ (dashed), $M = 5, \tau = 5$ (solid), $M = 2, \tau = 5$ (dash-dotted) and $M = 1, \tau = 5$ (dotted). Other parameter values are $h = 10^{-2}$ and $D = 1$.

$$M\frac{d^2\mathbf{u}_{0,\mathbf{m}}}{dt^2} = \sum_{|n_1'|\leqslant 1,|n_2-n_2'|\leqslant 1,|n_3-n_3'|\leqslant 1} \mathbf{C}_{(0,\mathbf{m})-\mathbf{n}'}\mathbf{u}_{\mathbf{n}'} + \mathbf{f}_{0,\mathbf{m}}. \tag{55}$$

Expressing $\mathbf{u}_{-1,\mathbf{m}'}$ as a function of $\mathbf{u}_{0,\mathbf{m}''}$ is enough to close the system. Due to the cross terms appearing in (49) it is not true in general that the odd extension $\mathbf{v}$ of $\mathbf{u}$ defined in (38) solves (49) with data obtained as odd extensions of the original data, as in (38)–(40). We must correct $\mathbf{g}_{n_1,\mathbf{m}}$ at $n_1 = 0$:

$$\mathbf{g}_{n_1,\mathbf{m}} = \begin{cases} \mathbf{f}_{n_1,\mathbf{m}} + \delta_{n_1,-1}\mathbf{a}_{\mathbf{m}}(t), & n_1 < 0 \\ \mathbf{b}_{\mathbf{m}}(t), & n_1 = 0 \\ -\mathbf{g}_{-n_1,\mathbf{m}}, & n_1 > 0 \end{cases} \tag{56}$$

$$\begin{aligned} \mathbf{a}_{\mathbf{m}}(t) &= \sum_{|n_2-n_2'|\leqslant 1,|n_3-n_3'|\leqslant 1} \mathbf{C}_{(-1,\mathbf{m})-(0,\mathbf{m}')}\mathbf{u}_{0,\mathbf{m}'}, \\ \mathbf{b}_{\mathbf{m}}(t) &= \sum_{|n_2-n_2'|\leqslant 1,|n_3-n_3'|\leqslant 1} [\mathbf{C}_{(0,\mathbf{m})-(-1,\mathbf{m}')} - \mathbf{C}_{(0,\mathbf{m})-(1,\mathbf{m}')}]\mathbf{u}_{-1,\mathbf{m}'}, \end{aligned} \tag{57}$$

where $\mathbf{m}' = (n_2', n_3')$. Solving the extended problem in the whole space with this new definition of $\mathbf{g}_{n_1,\mathbf{m}}$, we find $\mathbf{u}_{n_1,\mathbf{m}}, n_1 < 0$, as a function of $\mathbf{u}_{0,\mathbf{m}'}, \mathbf{u}_{-1,\mathbf{m}'}$:

$$\mathbf{u}_{n_1,\mathbf{m}}(t) = \int_0^t \sum_{\mathbf{m}'\in\mathbb{Z}^2} [\mathcal{G}_{\mathbf{n},(-1,\mathbf{m}')}(t-s)\mathbf{a}_{\mathbf{m}'}(s) + \mathcal{G}_{\mathbf{n},(0,\mathbf{m}')}(t-s)\mathbf{b}_{\mathbf{m}'}(s)]ds + \mathbf{r}_{n_1,\mathbf{m}}(t), \tag{58}$$

$$\mathbf{r}_{n_1,\mathbf{m}}(t) = \sum_{n_1'<0,\mathbf{m}'\in\mathbb{Z}^2} \left[\mathcal{G}_{\mathbf{n},\mathbf{n}'}(t)\frac{d\mathbf{u}_{\mathbf{n}'}}{dt}(0) + \frac{d\mathcal{G}_{\mathbf{n},\mathbf{n}'}}{dt}(t)\mathbf{u}_{\mathbf{n}'}(0) + \int_0^t \mathcal{G}_{\mathbf{n},\mathbf{n}'}(t-s)\mathbf{f}_{\mathbf{n}'}(s)ds\right], \tag{59}$$

where $\mathcal{G}_{\mathbf{n},\mathbf{n}'}, \mathbf{n} = (n_1, \mathbf{m})$, is the Green's function for the half-space $n_1 < 0$ with zero boundary condition on the wall. When $\mathbf{C}_{(0+1,\mathbf{m}-\mathbf{m}')} = \mathbf{C}_{(0-1,\mathbf{m}-\mathbf{m}')}, \mathbf{b}_{\mathbf{m}} = 0$ and (58) gives $\mathbf{u}_{-1,\mathbf{m}}$ as a function of $\mathbf{u}_{0,\mathbf{m}'}$, closing (55). Again, we have a boundary condition with the structure (37), (41), and (42). If $\mathbf{b}_{\mathbf{m}} \neq 0$, (58) involves values of $\mathbf{u}_{-1,\mathbf{m}'}$ in the interval $[0,t]$. Notice that $\mathcal{G}_{\mathbf{n},\mathbf{n}'}(0) = 0$. In practice, only known values of $\mathbf{u}_{-1,\mathbf{m}'}$ for times $s \in [0,t)$ are involved. This allows to compute $u_{-1,\mathbf{m}}(t)$ and close the truncated system in the half space $n_1 > 0$ as explained in the next subsection.

#### 4.2.3. Second order scheme

To solve (31) in the half-space $n_1 > 0$, we discretize the time derivatives appearing in the system (31) and the boundary condition (55) by means of (22). The integrals in (58) are discretized by the composite trapezoidal rule:

$$\mathbf{u}^j_{-1,\mathbf{m}} = \sum_{|n_2'|\leqslant N_2,|n_3'|\leqslant N_3} \sum_{i=0}^{j} \left[\mathcal{G}_{(-1,\mathbf{m}),(-1,\mathbf{m}')}(t_i)\mathbf{a}_{\mathbf{m}'}(t_j - t_i) + \mathcal{G}_{(-1,\mathbf{m}),(0,\mathbf{m}')}(t_i)\mathbf{b}_{\mathbf{m}'}(t_j - t_i)\right] + r_{-1,\mathbf{m}}(t_j). \tag{60}$$

The values $a_{\mathbf{m}'}(t_j)$ and $b_{\mathbf{m}'}(t_j)$ are not used because $\mathcal{G}_{\mathbf{n},\mathbf{n}'}(0) = 0$. Thus, $\mathbf{u}^j_{-1,\mathbf{m}}$ is expressed in terms of previously stored values: $u^i_{-1,\mathbf{m}'}$ and $u^i_{0,\mathbf{m}'}$ for $j < i$. In a finite box, we must truncate and shift (60) as explained in Section 4.1.3.

## 5. Conclusions

We have found nonreflecting boundary conditions for lattice models which include spatially discrete wave and Klein–Gordon equations. These boundary conditions may be extended to lattice models for general cubic crystals. Our boundary conditions are non local in time. We propose a discretization scheme which produces discretely absorbing boundary conditions. Numerical tests illustrate the ability of these boundary conditions to minimize reflections at boundary. They can either be used as artificial boundary conditions to truncate a computational domain or as transmission conditions to couple two domains with different dynamics and design hybrid multiscale schemes.

## Acknowledgments

Work supported by research grants FIS2008-04921-C02-02 and CM-910143.

## References

[1] S.A. Adelman, J.D. Doll, Generalized Langevin equation approach for atom/solid-surface scattering: General formulation for classical scattering off harmonic solids, J. Chem. Phys. 64 (1976) 2375–2388.
[2] A.R.A. Anderson, B.D. Sleeman, Wave front propagation and its failure in coupled systems of discrete bistable cells modelled by FitzHugh–Nagumo dynamics, Int. J. Bif. Chaos 5 (1995) 63–75.
[3] A. Appeló, G. Kreiss, A new absorbing layer for elastic waves, J. Comput. Phys. 215 (2006) 642–660.

[4] A. Arnold, M. Ehrhardt, Discrete transparent boundary conditions for wide angle parabolic equations in underwater acoustics, J. Comput. Phys. 145 (1998) 611–638.
[5] J. Bafalui, J.M. Rubi, The harmonic liquid away from equilibrium I and II, Phys. A 153 (1988) 129–159.
[6] A. Bayliss, E. Turkel, Radiation boundary conditions for wave-like equations, Commun. Pur. Appl. Math. XXXIII (1980) 707–725.
[7] A. Bayliss, E. Turkel, Far field boundary conditions for compressible flows, J. Comput. Phys. 48 (1982) 182–199.
[8] A. Bayliss, C.I. Goldstein, E. Turkel, On accuracy conditions for the numerical computation of waves, J. Comput. Phys. 59 (1985) 396–404.
[9] E. Beaches, S. Fauqueux, P. Joly, Stability of perfectly matched layers, group velocities and anisotropic waves, J. Comput. Phys. 188 (2003) 399–433.
[10] J.P. Berenger, A perfectly matched layer for the absorption of electromagnetic waves, J. Comput. Phys. 114 (1994) 185–200.
[11] L.L. Bonilla, Theory of nonlinear charge transport, wave propagation and self-oscillations in semiconductor superlattices, J. Phys. C 14 (2002) R341.
[12] W. Cai, M. Koning, V.V. Bulatov, S. Yip, Minimizing boundary reflections in coupled-domain simulations, Phys. Rev. Lett. 85 (2000) 3213–3216.
[13] A. Carpio, Nonlinear stability of oscillatory wave fronts in chains of coupled oscillators, Phys. Rev. E 67 (2004) 046601.
[14] P.M. Chaikin, T.C. Lubensky, Principles of condensed matter physics, Cambridge University Press, Cambridge, 1995 (Chapter 10).
[15] F. Collino, C. Tsogka, Application of the PML absorbing layer model to the linear elastodynamic problem in anisotropic heterogenous media, Geophysics 66 (2001) 294–307.
[16] P.A. Deymier, J.Q. Vasseur, Concurrent multiscale model of an atomic crystal coupled with elastic continua, Phys. Rev. B 66 (13) (2002) 134106.
[17] W. E, Z. Huang, A dynamic atomistic-continuum method for the simulation of crystalline materials, J. Comput. Phys. 182 (1) (2002) 234–261.
[18] W. E, Z. Huang, Matching conditions in atomistic-continuum modeling of materials, Phys. Rev. Lett. 85 (2001) 135501.
[19] B. Engquist, A. Majda, Absorbing boundary conditions for the numerical simulation of waves, Math. Comput. 31 (1977) 629–651.
[20] B. Engquist, A. Majda, Radiation boundary conditions for acoustic and elastic wave calculations, Commun. Pur. Appl. Math. 32 (1979) 312–358.
[21] J. Frenkel, T. Kontorova, On the theory of plastic deformation and twinning, J. Phys. USSR 13 (1938) 1–10.
[22] M.J. Grote, J.B. Keller, On nonreflecting boundary conditions, J. Comput. Phys. 122 (1995) 231–243.
[23] M.J. Grote, J.B. Keller, Nonreflecting boundary conditions for the time dependent wave equations, SIAM J. Appl. Math. 55 (2) (1995) 280–297.
[24] D. Givoli, I. Patlashenko, J.B. Keller, Discrete Dirichlet-to-Neumann maps for unbounded domains, Comput. Meth. Appl. Mech. Engrg. 164 (1998) 173–185.
[25] B. Gustafsson, Far-field boundary conditions for time-dependent hyperbolic problems, SIAM J. Sci. Statist. Comput. 9 (1988) 812–828.
[26] B. Gustafsson, Inhomogeneous conditions at open boundaries for wave propagation problems, Appl. Numer. Math. 4 (1988) 3–19.
[27] R.L. Higdon, Absorbing boundary conditions for difference approximations to the multidimensional wave equation, Math. Comput. 47 (1986) 437–459.
[28] R.L. Higdon, Radiation boundary conditions for dispersive waves, SIAM J. Numer. Anal. 31 (1994) 64–100.
[29] B.L. Holian, R. Ravelo, Fracture simulations using large scale molecular dynamics, Phys. Rev. B 51 (1995) 11275–11288.
[30] E.G. Karpov, G.J. Wagner, K.L. Wing, A Green's function approach to deriving nonreflecting boundary conditions in molecular dynamics simulations, Int. J. Numer. Meth. 62 (9) (2005) 1250–1262.
[31] J.P. Keener, J. Sneyd, Mathematical Physiology, Springer, New York, 1998.
[32] Ch. Lubich, A. Schaedle, Fast convolution for nonreflecting boundary conditions, SIAM J. Sci. Comput. 24 (2002) 161–182.
[33] M. Moseler, J. Nordiek, H. Haberland, Reduction of the reflected pressure wave in the molecular-dynamics simulation of energetic particle-solid collisions, Phys. Rev. B 56 (1997) 15439–15445.
[34] C.W. Rowley, T. Colonius, Discretely nonreflecting boundary conditions for linear hyperbolic systems, J. Comput. Phys. 157 (2000) 500–538.
[35] V.S. Ryaben'kii, S.V. Tsynkov, V.I. Turchaninov, Global discrete artificial boundary conditions for time-dependent wave propagation, J. Comput. Phys. 174 (2001) 712–758.
[36] J.M. Sanz-Serna, M.P. Calvo, Numerical hamiltonian problems, Applied Mathematics and Mathematical Computation, vol. 7, Chapman & Hall, 1994.
[37] F. Schmidt, D. Yevick, Transparent boundary conditions for Schrödinger-type equations, J. Comput. Phys. 134 (1997) 96–107.
[38] E. Schrödinger, The dynamics of elastically coupled point systems, Annalen der Physik 44 (1914) 916–934.
[39] B. Shiari, R.E. Miller, W.A. Curtin, Coupled atomistic/discrete dislocation simulations of nanoindentation at finite temperature, Trans. ASME 127 (2005) 358–368.
[40] L.I. Slepyan, Dynamics of a crack in a lattice, Sov. Phys. Dokl. 26 (1981) 538–540.
[41] L.N. Trefethen, L. Halpern, Well-posedness of one way wave equations and absorbing boundary conditions, Math. Comput. 47 (1986) 421–435.